Modelling of fracture occurrence in Ti6Al4V sheets at elevated temperature accounting for anisotropic behaviour

Qiaoling Wang , Stefania Bruschi , Andrea Ghiotti , Yanhong Mu

PII: S0020-7403(18)32175-1
DOI: https://doi.org/10.1016/j.ijmecsci.2018.10.045
Reference: MS 4601

To appear in: *International Journal of Mechanical Sciences*

Received date: 3 July 2018
Revised date: 22 October 2018
Accepted date: 22 October 2018

Please cite this article as: Qiaoling Wang , Stefania Bruschi , Andrea Ghiotti , Yanhong Mu , Modelling of fracture occurrence in Ti6Al4V sheets at elevated temperature accounting for anisotropic behaviour, *International Journal of Mechanical Sciences* (2018), doi: https://doi.org/10.1016/j.ijmecsci.2018.10.045

Highlights

- Ti6Al4V sheets fracture behaviour at room and elevated temperature affected by rolling direction and stress state.
- Barlat-Lian1989 and GISSMO models calibration through an extensive experimental campaign.
- Satisfactory prediction of fracture characteristics at varying rolling direction and temperature.

Modelling of fracture occurrence in Ti6Al4V sheets at elevated temperature accounting for anisotropic behaviour

Qiaoling. Wang[1,a], Stefania Bruschi[1,b*], Andrea Ghiotti[1,c], Yanhong. Mu[2,d]

[1]Department of Industrial Engineering, University of Padova, via Venezia 1, 35131 Padova, Italy.

[2]School of Mechanical Engineering, University of Science and Technology Beijing, 10083 Beijing, China

[a] qiaoling.wang@studenti.unipd.it , [b*] stefania.bruschi@unipd.it , [c] andrea.ghiotti@unipd.it , [d] muyanhong666@qq.com

Abstract:

The present research aims at modelling the fracture occurrence in Ti6Al4V titanium alloy sheets when deformed at room and elevated temperature, taking into account their anisotropic behaviour. The coupling of the Barlat-Lian 1989 anisotropic yield criterion and GISSMO damage model was introduced to predict the fracture occurrence and capture its anisotropic characteristics. The two models were calibrated on the basis of an extensive experimental campaign, including tensile tests on smooth and notched samples, shear tests and Nakajima-type tests at varying temperature and rolling direction. In order to validate the proposed approach, tests not used in the calibration phase were used, and the comparison between experimental and numerical results was carried out in terms of fracture characteristics at varying temperature and rolling direction. It was proved that the proposed modelling was able to satisfactorily reproduce the different fracture characteristics arising as a consequence of the sheet anisotropy and testing temperature.

Keywords: Ti6Al4V; sheet forming; damage; ductile fracture; anisotropy; elevated temperature

1. Introduction

Ti6Al4V titanium alloy is widely used in many industrial applications, such as biomedical, chemical, automotive and aerospace [1, 2], thanks to its high strength-to-weight ratio, excellent biocompatibility, elevated corrosion resistance, and low thermal expansion characteristics. Ti6Al4V is a biphasic alloy, with the dominant alpha phase at room temperature characterized by a Hexagonal Close-Packed (HCP) structure. The limited number of slip planes of HCP structures is known to lead to poor formability, which forces to form Ti6Al4V sheets at elevated temperature [3]. Furthermore, the limited number of slip planes induces a significant anisotropy of the material mechanical characteristics, which may also affect its failure behaviour. Ti6Al4V elasto-plastic behaviour taking into account the material anisotropy was mainly investigated at room temperature, as in [4] where different anisotropic yield criteria were calibrated through a series of tests performed on samples cut at different rolling directions. On the contrary, few literature records pertain to modelling of such behaviour at temperatures higher than the room temperature: an example is given in [5] where different anisotropic yield criteria were calibrated to simulate the deep drawing process conducted at 400°C on Ti6Al4V sheets. The same applies when modelling of damage evolution and fracture occurrence: scientific literature reports a few studies about the failure behaviour of titanium alloy sheets deformed at room temperature [6], taking into account the anisotropic behaviour on the basis of the plasticity model, whereas the possible anisotropic failure behaviour at elevated temperature hasn't been reported yet. To this aim, it is mandatory: i) to evaluate to which extent damage and fracture show anisotropic characteristics at varying temperature, and ii) to provide a damage evolution model capable to capture the influence of the sheet rolling direction on failure at varying temperature.

Within the numerous models available in literature to model damage evolution and fracture occurrence, the phenomenological ones appear the most suited thanks to their inherent easiness in implementation into commercial

Finite Element (FE)-based codes devoted to simulation of sheet forming processes and readiness of calibration [7]. In this paper, the phenomenological damage model called GISSMO (Generalized Incremental Stress State dependent MOdel) is applied to predict the onset of failure, taking into account the influence of the material anisotropy. The GISSMO model takes into account the dependence of the stress state through the stress triaxiality, whereas the Lode angle dependence is not considered, as shell elements are usually utilized when simulating sheet forming operations. The GISSMO model has been extensively used to predict failure of metals at room temperature: in [8], dual-phase steel sheets were formed and later on subjected to crash loading conditions and their failure behaviour analysed; in [9], the model was applied to martensitic steel sheets under various stress state, whereas in [10] the comparison between the predictions of the GISSMO model and those of a fracture criterion based on fracture forming limits proved that the former was more accurate; in [11], it was proved that the GISSMO model reduced significantly the simulation time compared to other fracture criteria, being still capable of satisfactory prediction of the material failure.

In this framework, the aim of the paper is to analyse and numerically model the Ti6Al4V sheets failure behaviour at varying temperature and specimen rolling direction. An extensive experimental campaign was carried out to calibrate and validate the chosen yield criterion and failure model, including tensile tests on smooth and notched specimens, shear tests and Nakajima-type tests at varying temperature and rolling direction. The results of the experimental campaign are presented in Section 2 of the paper, whereas Section 3 pertains to the description of the numerical models developed to simulate the experiments, in which the calibrated yield criterion and damage model were implemented. Section 4 shows the calibration procedure of the employed models and related results, as well as the validation cases are presented.

2. Experimental

Ti6Al4V titanium alloy sheets with a thickness of 1 mm were selected as testing material, from which the specimens used in the experimental campaign were laser cut. Tensile tests on smooth and notched samples, shear tests and Nakajima-type tests were carried out to cover a wide range of stress triaxiality, between simple shear and equi-biaxial tension, to both calibrate and validate the models used to describe the elasto-plastic and fracture behaviour of the Ti6Al4V sheets deformed at room and elevated temperature. These tests allowed evaluating the flow behaviour, anisotropic and fracture characteristics at varying temperature, strain rate and rolling direction.

2.1 Tensile tests on smooth specimens

Uniaxial tensile tests were carried out according to the ASTM E8/E8M-16a standard [12] using smooth specimens machined with a gauge length of 65 mm. The tensile tests were conducted on a universal 5 t MTS™ testing machine equipped with a resistance heating system to heat up the specimen to the testing temperature. After 30 s of soaking time at the testing temperature to homogenise the thermal field, the specimens were strained until fracture and left to cool in calm air to room temperature. The Aramis™ system from GOM was used to capture the strain field evolution of the specimen during deformation till fracture. In order to record the strain evolution, a thin layer of white and black paint speckle patterns was applied on one side of the specimen. The Aramis™ recorded data were also used to calculate the Lankford coefficients, namely the plastic anisotropy coefficients, on the basis of the width and thickness strain values.

The experimental set-up used for tensile testing is shown in Figure 1 (a). The testing temperatures were chosen from room temperature to 800°C, applying strain rates of 0.01, 0.1, 1 s^{-1} in order to identify the material behaviour sensitivity to temperature and strain rate. These values of testing temperature and strain rate are within the ranges of those applicable in forming of titanium alloy sheets.

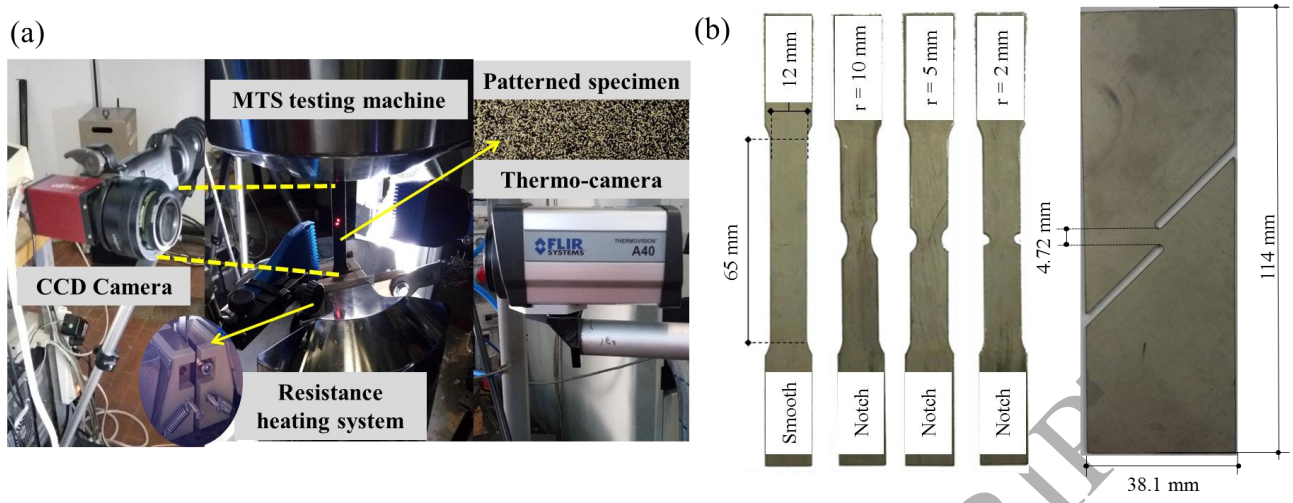

Fig. 1 (a) Experimental set-up, and (b) specimens used for tensile and shear testing.

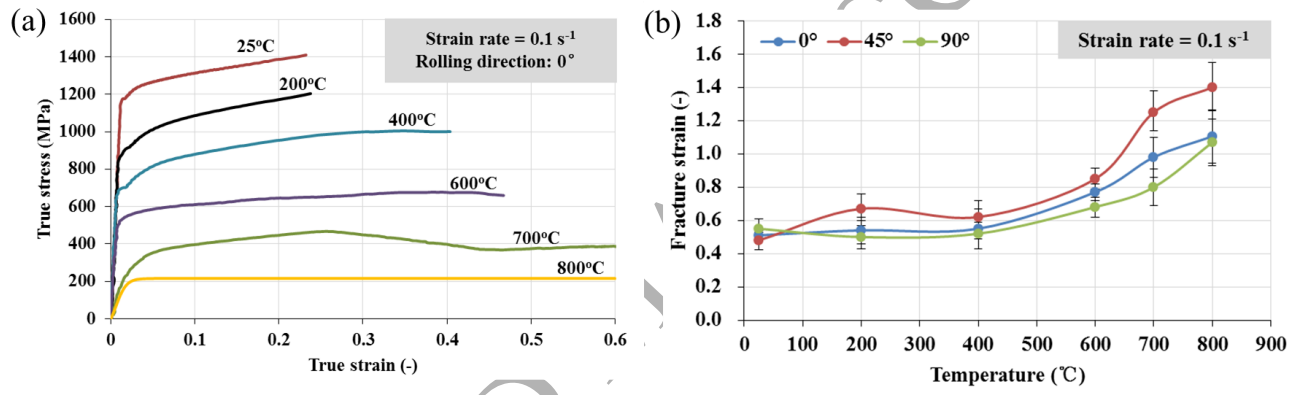

Fig. 2 (a) Flow behaviour at varying temperature, and (b) fracture strain at varying temperature and specimen rolling direction.

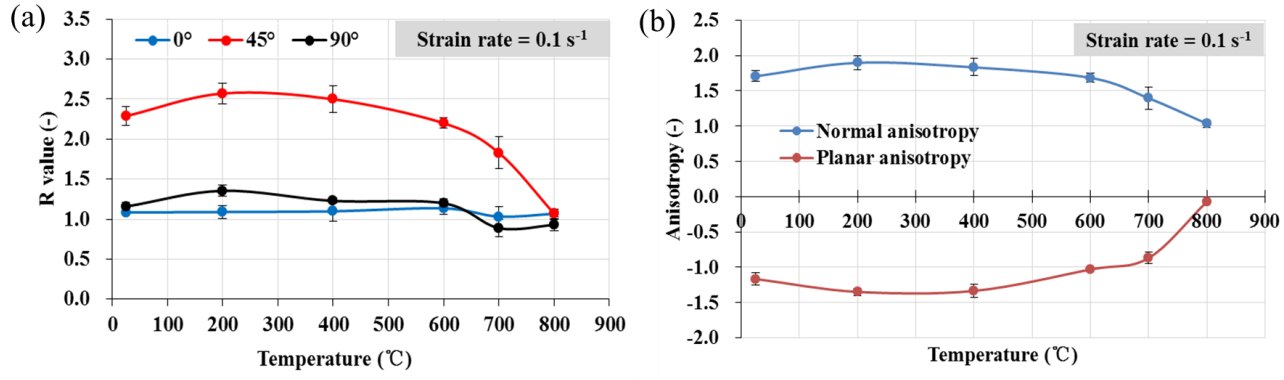

Fig. 3 (a) Lankford coefficients, and (b) average normal and planar anisotropy at varying temperature.

Figure 2 (a) shows the high flow stress sensitivity to temperature at strain rate of 0.1 s^{-1} for specimens cut at 0° with respect to the rolling direction. Figure 2 (b) reports the strain at fracture as a function of the testing temperature and specimen rolling direction: in general, a significant increase of ductility is seen starting from 600°C, identifying this temperature as the one at which the benefit of elevated temperature forming in terms of enhanced formability can

be exploited. Furthermore, there is a remarkable sensitivity to the rolling direction, as specimens cut at 45° with respect to the rolling direction always show the highest ductility, whereas specimens cut at 90° always the lowest, regardless of the testing temperature. The temperature influence on the Lankford coefficients and on the average normal and planar anisotropy is reported in Figure 3 (a) and Figure 3 (b), respectively: a similar anisotropic behaviour pertains to temperature up to 600°C, which gradually reduces to disappear at 800°C. This behaviour can be ascribed to the increase of beta phase volume fraction at increasing temperature, which becomes significant at temperature above 600°C [13]. In fact, there is a gradual change from the Hexagonal Closed Packed (HCP) crystal structure, typical of the alpha phase and characterized by a limited number of slip planes as well as high anisotropy, to the Body Centred Cubic (BCC) structure, typical of the beta phase and characterized by a much higher number of slip planes and reduced anisotropy. This change in the crystal structure is responsible of both the higher ductility and more isotropic behaviour close to 800°C. It is worth noticing that the highest values of Lankford coefficients pertain to specimens cut at 45° with respect to the rolling direction, which show to provide the highest ductility, regardless of the testing temperature. Similar results were obtained for the other strain rates and not here reported.

2.2 Tensile tests on notched specimens and shear tests

In order to have various stress states, tensile tests on notched specimens and shear tests were also carried out, using the same experimental apparatus and procedure described in §2.1. The notch radii were chosen equal to 2, 5 and 10 mm, whereas the shear specimens were machined according to the ASTM B831 standard [14] (see geometries in Figure 1 (b)). These tests were carried out at room temperature and 600°C, being the latter the temperature at which a remarkable change of material behaviour was found (see results in §2.1) and, therefore, chosen for forming Ti6Al4V sheets at elevated temperature. The strain rate was set equal to 0.1 s^{-1}. All the tests were carried out at varying rolling direction in order to assess the anisotropy influence on the strain at fracture at varying stress state. The strain at fracture of the notched samples was determined on the basis of the Aramis™ data, whereas the procedure described in [15] was adopted for evaluating the strain at fracture after shear testing. The stress state was identified in terms of stress triaxiality η according to Equation (1) where σ_m is the hydrostatic stress, and $\bar{\sigma}$ the Von Mises equivalent stress.

$$\eta = \frac{\sigma_m}{\bar{\sigma}} \tag{1}$$

The value of stress triaxiality for each test was determined on the basis of numerical simulations of the tests themselves. Details can be found in [15].

For the calibration of the damage model reported in §4, the values of the instability strain were also evaluated, namely the values of strain at Ultimate Tensile Stress (UTS) recorded from the experimental engineering stress-strain curves [16].

2.3 Nakajima-type tests

Nakajima tests were carried out at room temperature and 600°C, using an average strain rate of 0.1 s^{-1}, according to the procedure reported in the ISO 12004 standard [17]. The Nakajima testing set-up is shown in Figure 4 (a): it consists of a hemispherical punch (100 mm dia.) and a blank holder, mounted on a 200 kN hydraulic testing device. A 0.1 mm thick graphite foil is used as lubricant between the sheet metal specimen and the punch to reduce friction as much as possible. Cartridge heaters are inserted in the hemispherical punch to keep the temperature of the specimen during the experiments constant and equal to the testing temperature. An induction heating coil is used to heat up the specimen to the target temperature, which is continuously monitored through three K-type

thermocouples spot-welded at the centre, intermediate and outer diameter of the specimen surface deformed by the punch. Two stereoscopic CCD cameras were used to monitor the specimen deformation during the test and the Aramis™ system allowed determining the major and minor strain values. Two specimen geometries were selected to be tested under Nakajima-type test conditions, namely a round specimen of 210 mm diameter and a 100 mm wide notched specimen (see geometries in Figure 4 (b)). The former was used for calibrating the damage model giving rise to an equi-biaxial state of stress, whereas the latter for validating the model at varying rolling direction. The fracture strain values were recorded from the Aramis™ data.

The whole experimental plan, comprising tensile tests on smooth and notched samples, shear tests and Nakajima tests, is reported in Table 1.

Table 2 and Table 3 reports the values of strain at fracture and instability strain at varying stress triaxiality and specimen rolling direction at room temperature and 600°C, respectively. It is worth underlining that instability strain values are not reported in case of shear samples, as the simple shear fracture occurs without necking.

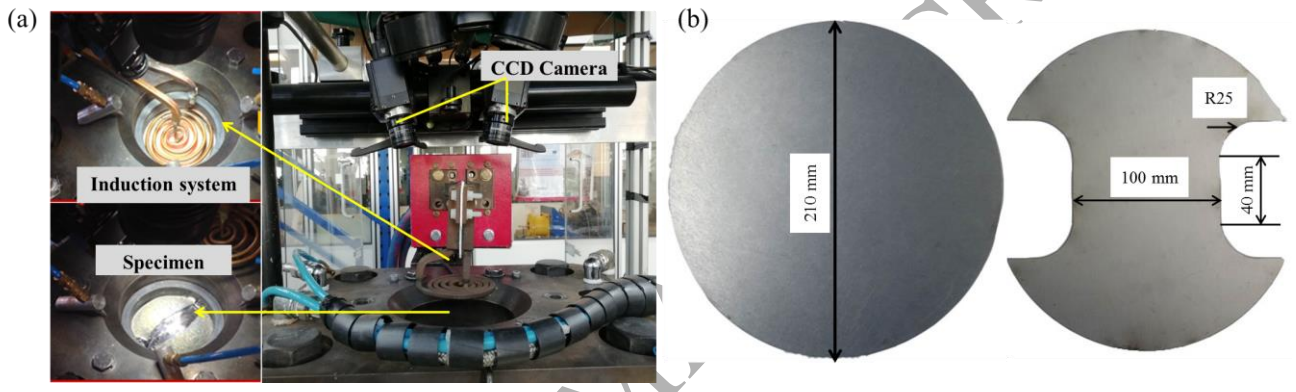

Fig. 4 (a) Experimental set-up, and (b) specimens used for Nakajima testing.

Table 1 Experimental plan.

Specimen	Temperature (°C)						Strain rate (s^{-1})	Rolling direction (-)
2 mm notched	25			600			0.1	0°, 45°, 90°
5 mm notched	25			600			0.1	0°, 45°, 90°
10 mm notched	25			600			0.1	0°, 45°, 90°
shear	25			600			0.1	0°, 45°, 90°
Nakajima round	25			600			0.1	-
Nakajima notched	25			600			0.1	0°, 45°, 90°
smooth	25	200	400	600	700	800	0.01, 0.1, 1	0°, 45°, 90°

Table 2 Fracture and instability strain values at room temperature at varying stress triaxiality and specimen rolling direction.

T=25℃ $\dot{\varepsilon}$ =0.1s^{-1}	η	0°		45°		90°	
		ε_f	ε_{inst}	ε_f	ε_{inst}	ε_f	ε_{inst}
shear	0.11	0.733	-	0.454	-	0.9	-
smooth	0.34	0.51	0.101	0.48	0.07	0.55	0.085
10 mm notched	0.42	0.43	0.0177	0.45	0.016	0.42	0.017
5 mm notched	0.47	0.35	0.0185	0.36	0.018	0.36	0.0172

2 mm notched	0.52	0.34	0.0194	0.35	0.0191	0.35	0.0164
Nakajima round	0.66	0.38	0.05	0.38	0.05	0.38	0.05

Table 3 Fracture and instability strain values at 600°C at varying stress triaxiality and specimen rolling direction.

T=600℃ $\dot{\varepsilon}$ **=0.1s^{-1}**	η	**0°**		**45°**		**90°**	
		ε_f	ε_{inst}	ε_f	ε_{inst}	ε_f	ε_{inst}
shear	0.11	1.134	-	1.012	-	1.274	-
smooth	0.34	0.77	0.125	0.85	0.176	0.68	0.09
10 mm notched	0.42	0.68	0.062	0.72	0.085	0.65	0.052
5 mm notched	0.47	0.64	0.07	0.66	0.097	0.62	0.052
2 mm notched	0.52	0.6	0.072	0.64	0.099	0.59	0.053
Nakajima round	0.66	0.66	0.13	0.66	0.13	0.66	0.13

3. Numerical modelling of the tests

The thermo-mechanically coupled numerical models of the tests described in §2 were developed with the Ls-Dyna™ code version R9.1.0 (Ls_Prepost V4.5), using a dynamic-implicit analysis. The specimens were discretized using shell elements of 1 mm of thickness with 5 through-thickness integration points. After a preliminary sensitivity analysis, the element size was set less than 0.5 mm in the deformation zone to avoid any influence on damage prediction. The dies simulated for the Nakajima set-up were considered rigid.

In case of tensile and shear tests models, the specimen testing temperature was simulated implementing a localized heat generation source to the sample central zone on the basis of recordings of an infrared thermo-camera (see Figure 5 (a)); whereas, in case of Nakajima tests models, the initial thermal field of the specimen was simulated with the same dimensions of the inductor heads used for heating up (see Figure 5 (b)). Graphite foils were used as lubricant, using static and dynamic friction coefficients between the punch and specimen equal to 0.1 and 0.05 at room temperature, respectively, while at 600°C the same values were set equal to 0.2 and 0.1 [18,19].

Temperature-dependent values of the Young's modulus, Poisson's ratio, heat capacity and thermal conductivity were implemented [20], whereas the density was kept constant (see Table 4).

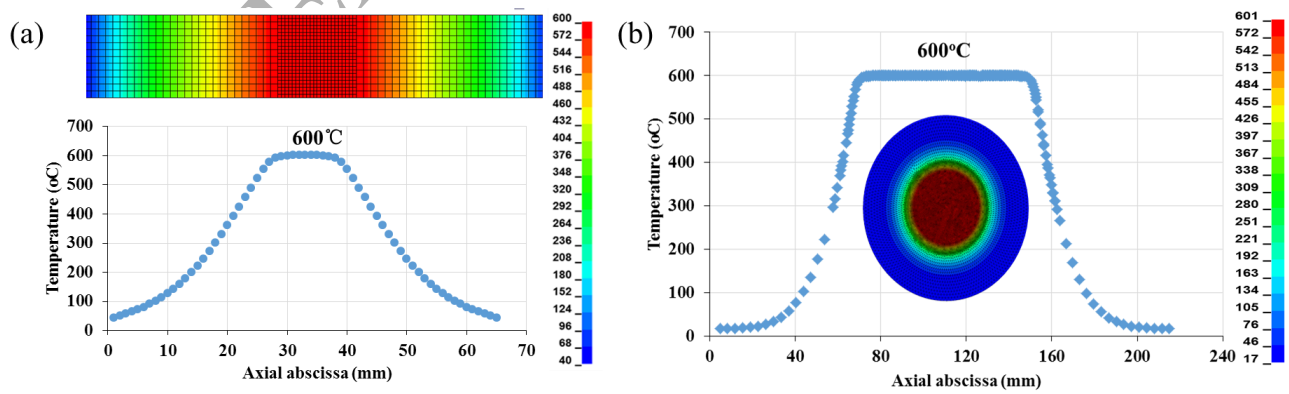

Fig. 5 Temperature distribution implemented in case of tensile test on smooth specimens (a) and in case of Nakajima test on round specimens (b).

Table 4 Ti6Al4V mechanical and thermo-physical properties implemented at room temperature and 600°C [20].

	Density (g/cm^3)	Young's modulus (GPa)	Poisson's ratio (−)	Heat capacity (J/kgK)	Thermal conductivity (W/mK)
T = 25°C	4.54	105	0.23	580	6.65
T = 600°C		74.2	0.24	725	14.7

4. Damage modelling accounting for anisotropic behaviour

The influence of the sheet anisotropy was taken into account in both the yield criterion and hardening rule used to model the material elasto-plastic behaviour as well as the damage model used to predict the fracture onset. In the following paragraphs the main features of the employed yield criterion and damage model are presented together with the calibration procedure.

4.1 Barlat-Lian1989 yield criterion and hardening rule

The anisotropic yield locus at room temperature and 600°C was modelled using the Barlat-Lian 1989 yield criterion [21], developed for materials exhibiting planar anisotropy, as is the case of Ti6Al4V (see Figure 3 (b)), based on the following formulation:

$$f = a|k_1 + k_2|^M + a|k_1 - k_2|^M + c|2k_2|^M = 2\sigma_e^M \quad (2)$$

where *k1* and *k2* are invariants of the stress tensor, *M* is an integer exponent, which is related to the crystallographic structure of the material, and σ_e is the effective stress.

The constants *a*, *c* ad *h* are calculated on the basis of the following equations:

$$k_1 = \frac{\sigma_{11}+h\sigma_{22}}{2}, \quad k_2 = \left[\left(\frac{\sigma_{11}-h\sigma_{22}}{2}\right) + p^2\sigma_{12}^2\right]^{1/2} \quad (3)$$

$$a = 2 - c = 2 - 2\sqrt{\frac{r_0}{1+r_0}\cdot\frac{r_{90}}{1+r_{90}}} \quad (4)$$

$$h = \sqrt{\frac{r_0}{1+r_0}\cdot\frac{1+r_{90}}{r_{90}}} \quad (5)$$

where r_0, r_{45}, r_{90} are the three Lankford coefficients.

Compared to other yield criteria usually implemented for the numerical simulation of sheet forming processes, the calibration of this yield criterion requires a low number of material constants, namely the three Lankford coefficients r_0, r_{45}, r_{90} and the constant *M* that depends on the alloy crystallographic structure. The former were implemented on the basis of the tensile tests on smooth samples reported in §2, whereas the latter was chosen equal to 12 as reported in [4] for HCP metals at room temperature. It is worth underlining that the same value of *M* was used at 600°C since the HCP crystal lattice is still the dominating structure at this temperature, as the phase transformation into a BCC structure is almost negligible at 600°C [13].

Among other yield criteria, the Barlat-Lian 1989 criterion was also chosen as, in a previous work by the Authors [22], it was found suitable to accurately predict the strain localization due to plastic instability, which is mandatory for a proper calibration of the damage model described in the following.

The associated flow rule was implemented by using the experimental flow curves derived from specimens oriented at 0° at varying temperature and strain rate to account for strain hardening, temperature and strain rate sensitivity.

4.2. GISSMO model

The Generalized Incremental Stress State dependent damage MOdel (GISSMO model hereafter), developed by

Neukamm et al [23], predicts damage evolution and fracture occurrence in ductile metals using a phenomenological approach. The model combines an incremental damage accumulation formulation, based on a failure curve function of the actual stress state, with an incremental instability accumulation formulation, based on a critical strain curve, again function of the actual stress state. The accumulated damage D and the so-called instability measure F are computed according to Equations (6) and (7), respectively.

$$\mathrm{D}D = \frac{n}{e_f(h)} D^{\left(1-\frac{1}{n}\right)} \mathrm{D}e_u \tag{6}$$

$$\mathrm{D}F = \frac{n}{e_{inst}(h)} F^{\left(1-\frac{1}{n}\right)} \mathrm{D}e_u \tag{7}$$

Here, $\Delta\varepsilon_v$ is the actual equivalent plastic strain increment, n is a damage exponent that accounts for a non-linear relationship between strain and damage, which is reasonable since damage is expected to accelerate when approaching failure, $e_f(h)$ and $e_{inst}(h)$ are the fracture strain and instability strain as function of the stress triaxiality, respectively. Failure occurs when the damage D reaches unity. On the other hand, when the instability measure is equal to 1, which means strain localization occurs, with the accumulated damage that reaches a critical value D_{crit}, the accumulated damage affects the stress σ according to Equation (8).

$$\sigma = \tilde{\sigma}\left[1-\left(\frac{D-D_{crit}}{1-D_{crit}}\right)^m\right] \tag{8}$$

where m is an exponent for damage related stress fadeout.

4.3 Calibration of the GISSMO model

For calibrating the GISSMO model, the curves of fracture strain ε_f and instability strain ε_{inst} vs. stress triaxiality η as well as the fading exponent m and the damage exponent n are needed. Figure 6 reports the former curves as a function of the specimen rolling direction at room temperature and 600°C. A significant influence of the rolling direction is appreciable, with the 45° direction showing always a higher ductility in case of smooth, notched and Nakajima round specimens whereas a ductility increase is shown by the 90° direction in case of shear testing, regardless of the testing temperature.

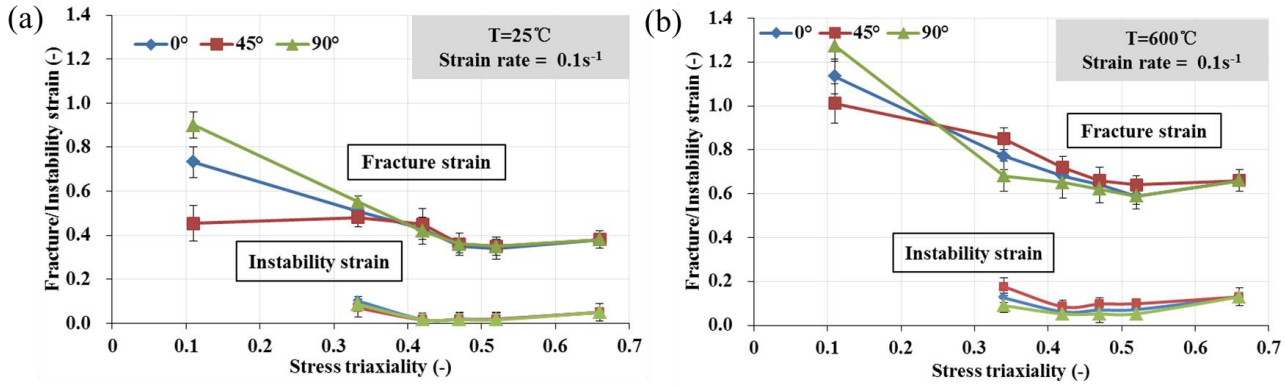

Fig. 6 Fracture and instability strain curves as a function of the stress triaxiality and specimen rolling direction at (a) room temperature, and (b) 600℃.

The two exponents *m* and *n* were identified using the LS-OPT^{TM} optimization software on the basis of the Sequential Response Surface Method (SRSM) [24,25], whose procedure consists in varying the two exponents until the mismatch between the experimental and computed force vs. displacement curves is small enough. The experimental force vs. displacement curves chosen for the optimization procedure were the ones from the tensile tests carried out on smooth specimens at different rolling directions at 600°C, which were compared with the ones calculated by the related numerical models where the curves of Figure 6 (b) were implemented. The so-called Curve Mapping algorithm (which computes the area between the curves and the x-axis) was used for optimization, as is especially suitable in this case where the force vs. displacement curves are characterized by a significant drop just before failure. The flow chart showing the optimization procedure is reported in Figure 7. After a few iterations, the damage exponent *n* was identified equal to 4 and the fading exponent *m* equal to 1.5. The same values were also suitable for the other testing conditions, therefore any further optimization was neglected.

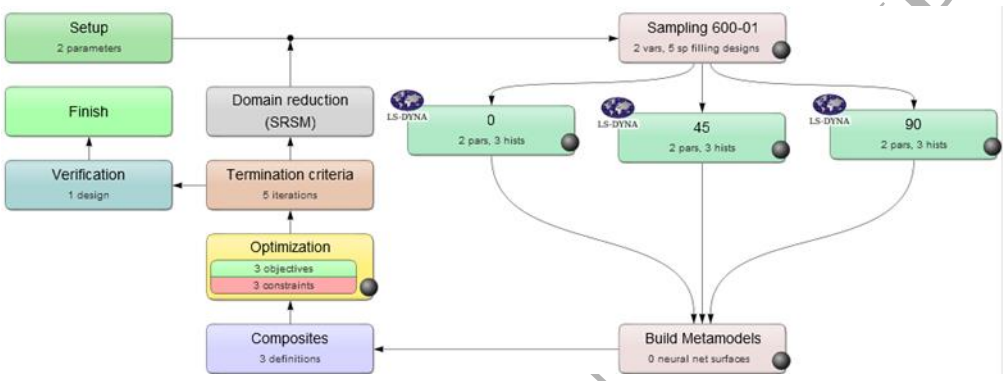

Fig. 7 Flow chart of the optimization procedure to identify the damage and fading exponents of the GISSMO model.

The comparison between the fracture characteristics predicted by the numerical models of the tests calibrated on the basis of the above described procedure and the experimental ones is shown from Figure 8 to Figure 15, which are relevant to tests carried out at room temperature and 600°C on specimens oriented at 0°, 45° and 90° with respect to the rolling direction. In case of tensile and shear tests, the comparison was carried out considering the strain field just before fracture, the shape of the fracture, and the force vs. displacement curve. In case of Nakajima tests conducted on round specimens, the comparison was about the shape of the fracture and the height of the fractured dome.

Figure 8, relevant to smooth specimens deformed at room temperature, shows a good agreement between experimental and numerical results, regardless of the specimen rolling direction. In case of 5 mm notched specimens deformed at room temperature, the agreement is still very satisfactory when testing the 0° and 45° rolling direction, with the 90° specimen showing a simulated fracture that is anticipated of approximately 9.5% compared to the experimental one, but with again a good prediction of the fracture shape. Similar results were obtained for the other notched specimens, and therefore not here reported. In case of shear specimens deformed at room temperature, the model is again capable to catch the fracture shape, but the fracture occurrence is overestimated for the 90° rolling direction of about 20%, even if the shape of the curve final portion is well represented. At room temperature, it is worth noting that the highest ductility shown by the 0° smooth specimen and the 45° notched specimen is well predicted, as is the highest ductility in case of 90° shear specimen. As shown in Figures 9 and 10, the strain field is well predicted for the 90° rolling direction of the smooth specimen, whereas the simulated fracture is less accurate for the 90° rolling direction of both the notched and shear specimens.

The comparison between experimental and numerically predicted fracture characteristics in case of Nakajima round specimens deformed at room temperature is shown in Figure 11: both the fracture shape and the height of the

fractured dome are well predicted.

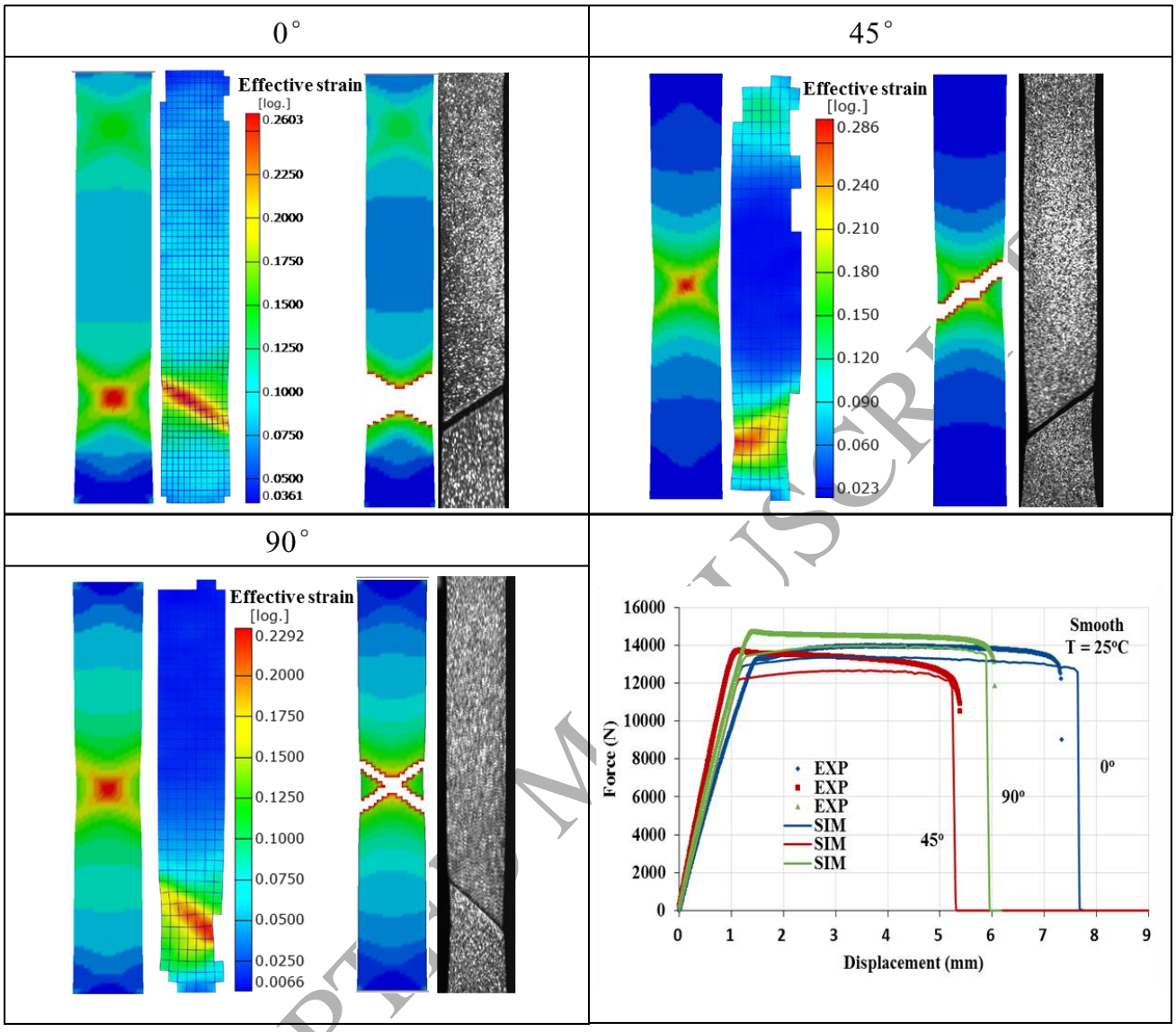

Fig. 8 Experimental and numerically predicted fracture characteristics of smooth specimens deformed at room temperature at varying rolling direction.

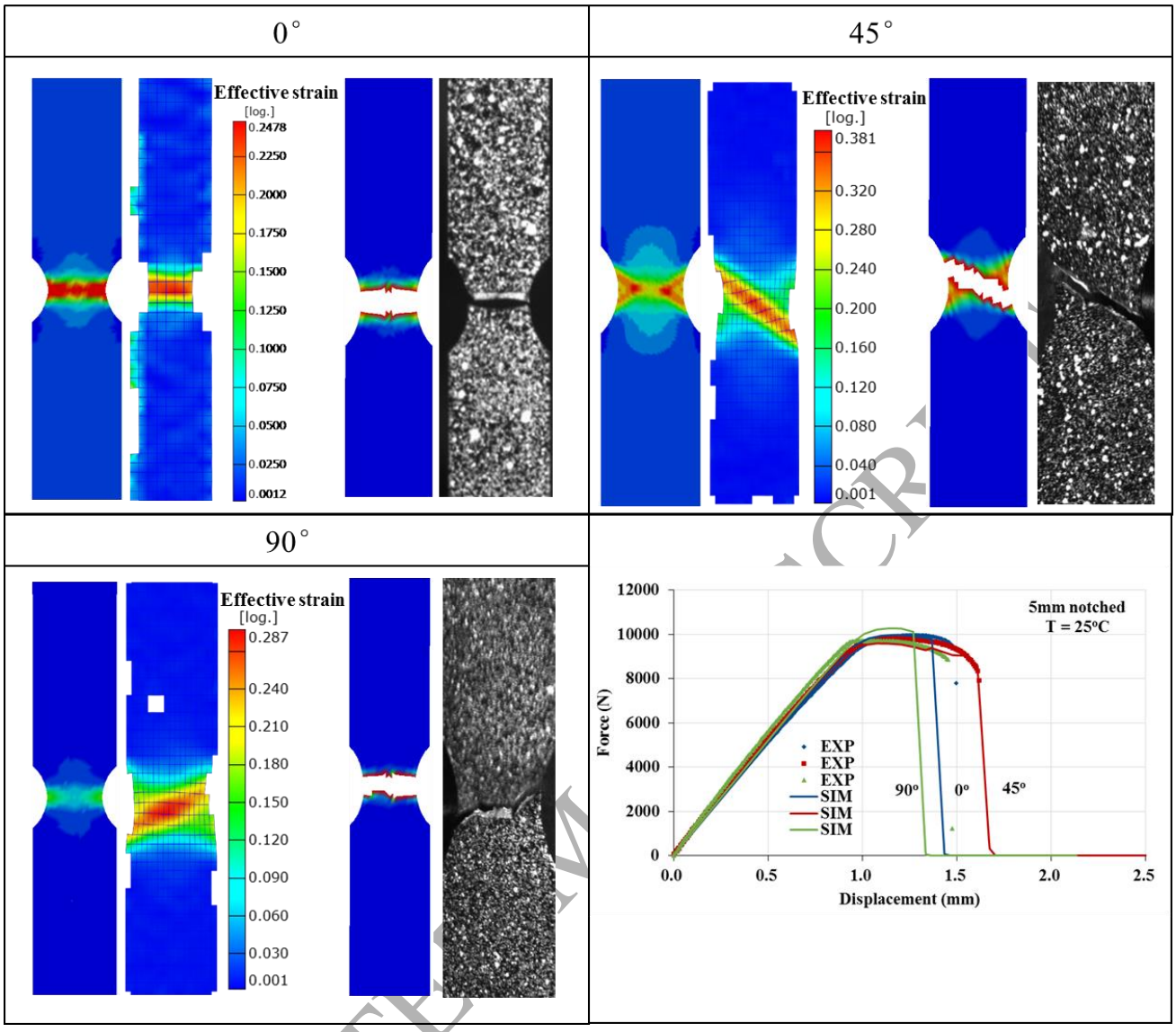

Fig. 9 Experimental and numerically predicted fracture characteristics of 5 mm notched specimens deformed at room temperature at varying rolling direction.

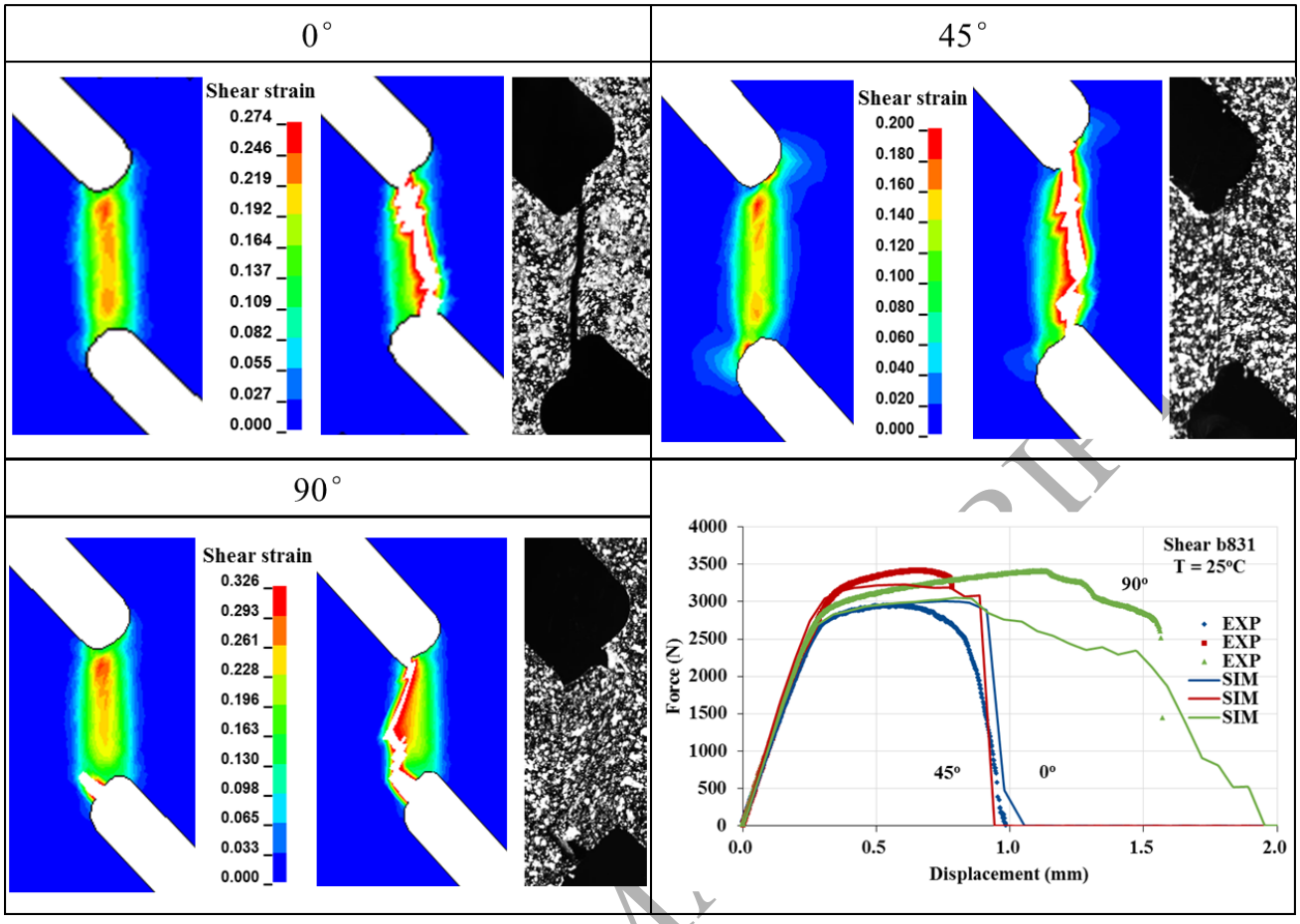

Fig. 10 Experimental and numerically predicted fracture characteristics of shear specimens deformed at room temperature at varying rolling direction.

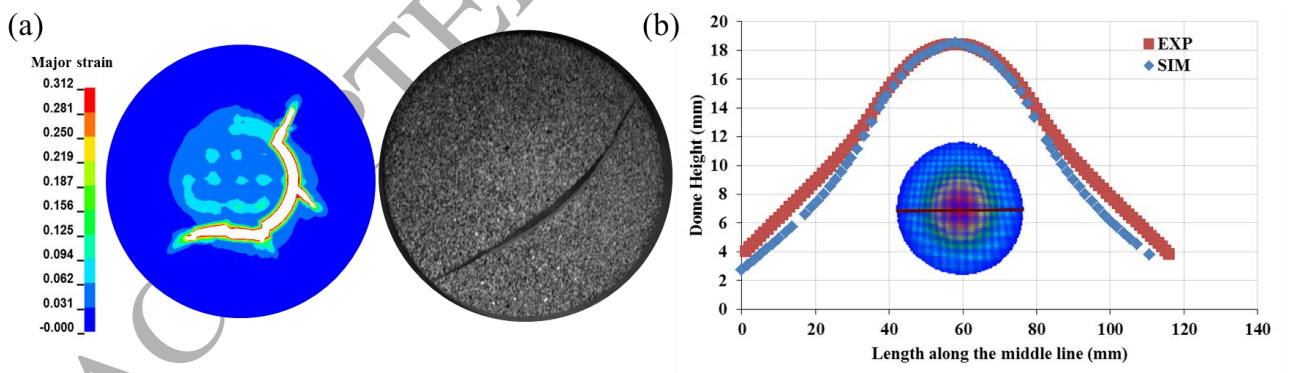

Fig. 11 Experimental and numerically predicted fracture characteristics of Nakajima round specimens deformed at room temperature.

At 600°C, the fracture characteristics change as a consequence of the material higher ductility. In case of smooth specimens, as shown in Figure 12, the strain field is well predicted for the 0° and 45° directions, whereas the experimental strain localization for the 90° agrees less with the numerical outcome. On the contrary, the prediction of the fracture shape is very good for all the three directions: especially at 45° direction even the location of the fracture onset at the middle of the specimen is correctly reproduced by the numerical model, as well as the force vs.

displacement curves. In case of 5 mm notched specimens, as shown in Figure 13, the model is able to catch the fracture occurrence at the edge of the specimens and the almost flat fracture shape regardless of the specimen rolling direction. At 90° direction, the numerical force vs. displacement curve differs of about 18% from the experimental one in terms of displacement at fracture, whereas the other two directions are well predicted, as is the case at room temperature. Similar results were obtained for the other notched specimens, and therefore not here reported. In case of shear specimens, as shown in Figure 14, regardless of the rolling direction, the numerically predicted fracture shape tilts on the left differently from the experimental fractures that tilt on the right. Contrary to room temperature testing, the experimental and numerical force vs. displacement curves relevant to 0° direction differ of about 17% in the displacement at fracture. It is worth underlining that the highest ductility shown by the 45° smooth and notched specimens is always predicted, as is predicted the highest ductility shown by the 90° specimens under shear testing conditions.

Again, the good agreement between experimental and numerical fracture shapes and positions in the Nakajima round specimen is seen in Figure 15 when testing at 600°C.

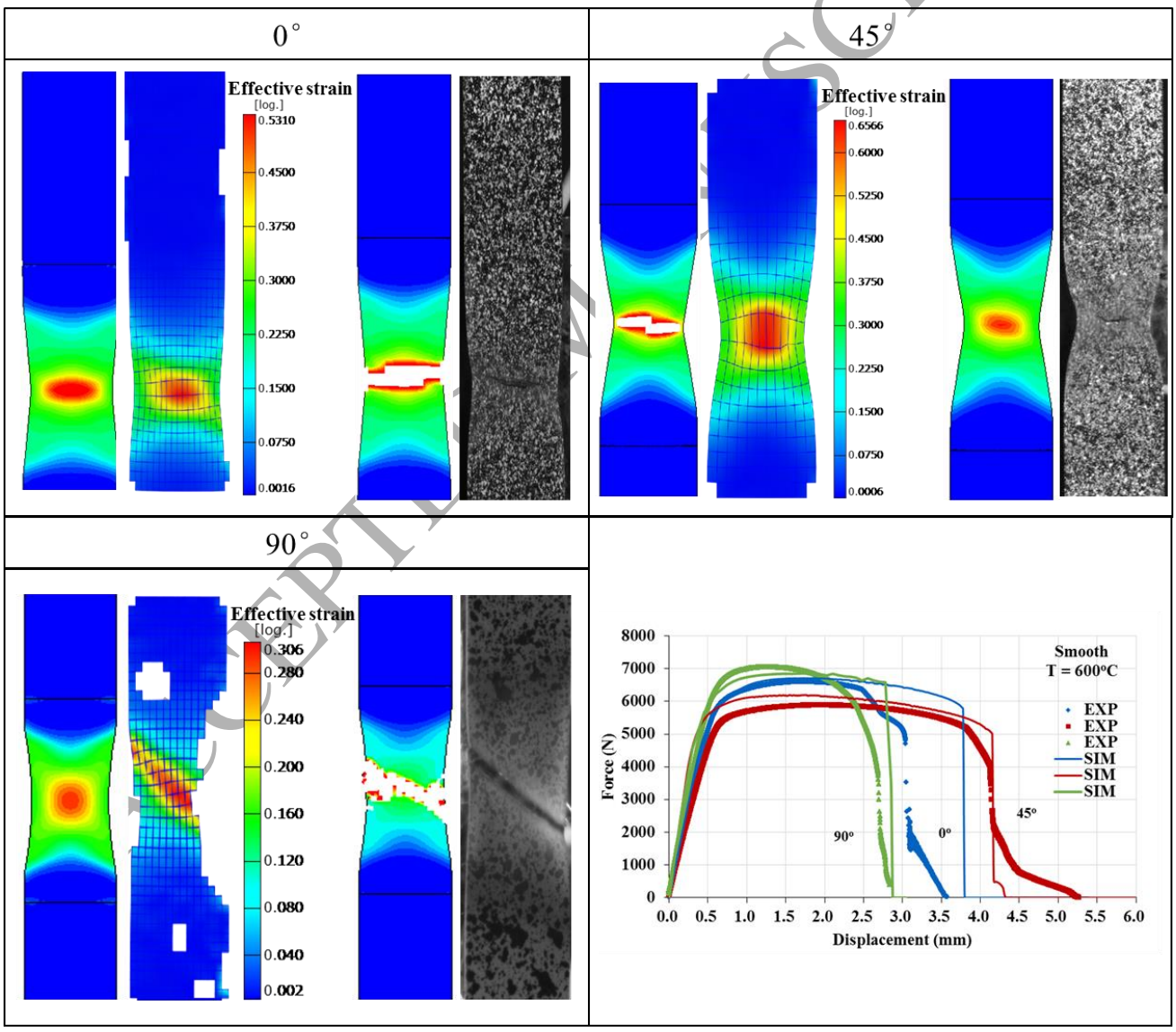

Fig. 12 Experimental and numerically predicted fracture characteristics of smooth specimens deformed at 600°C at varying rolling direction.

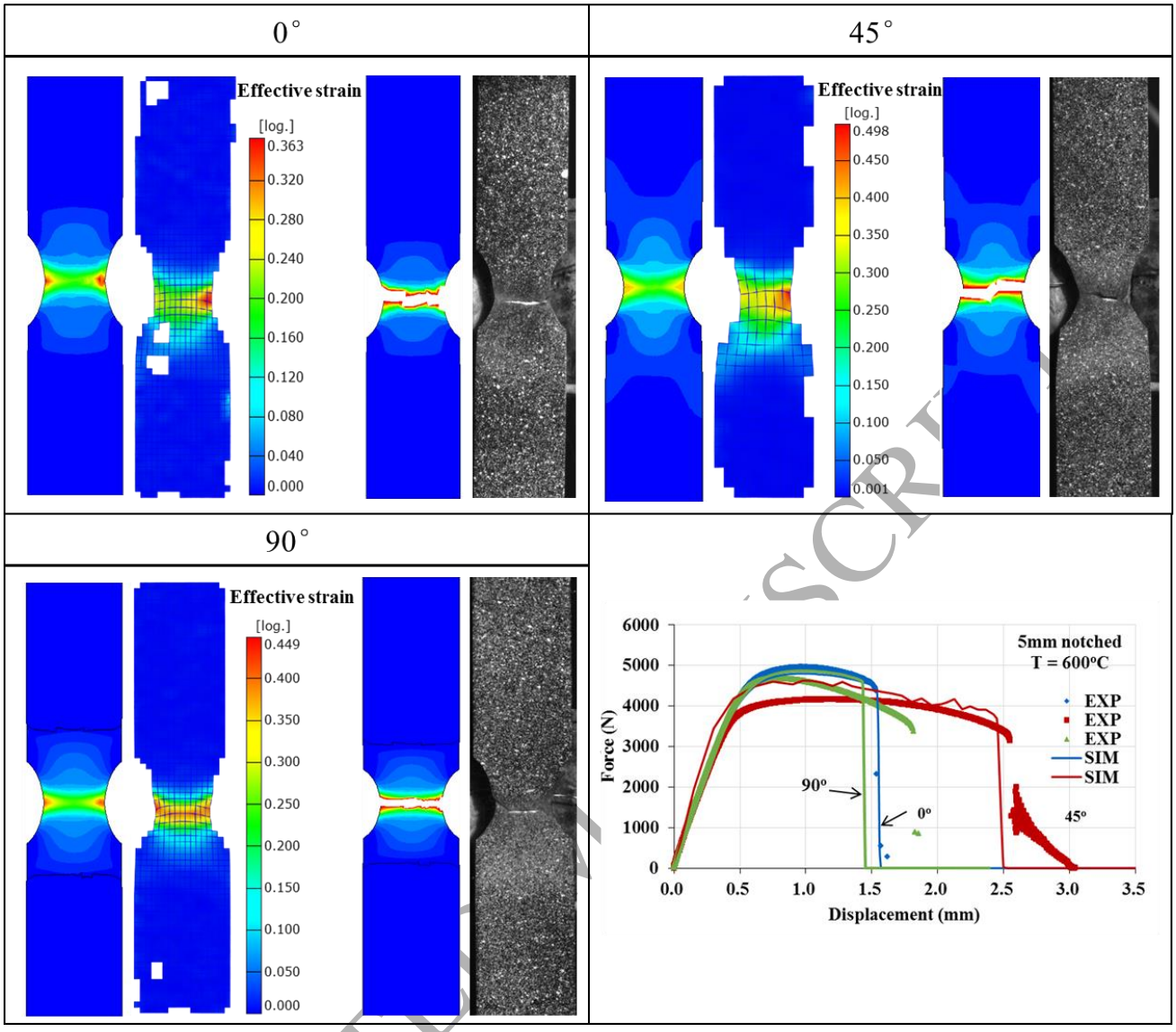

Fig. 13 Experimental and numerically predicted fracture characteristics of 5 mm notched specimens deformed at 600°C at varying rolling direction.

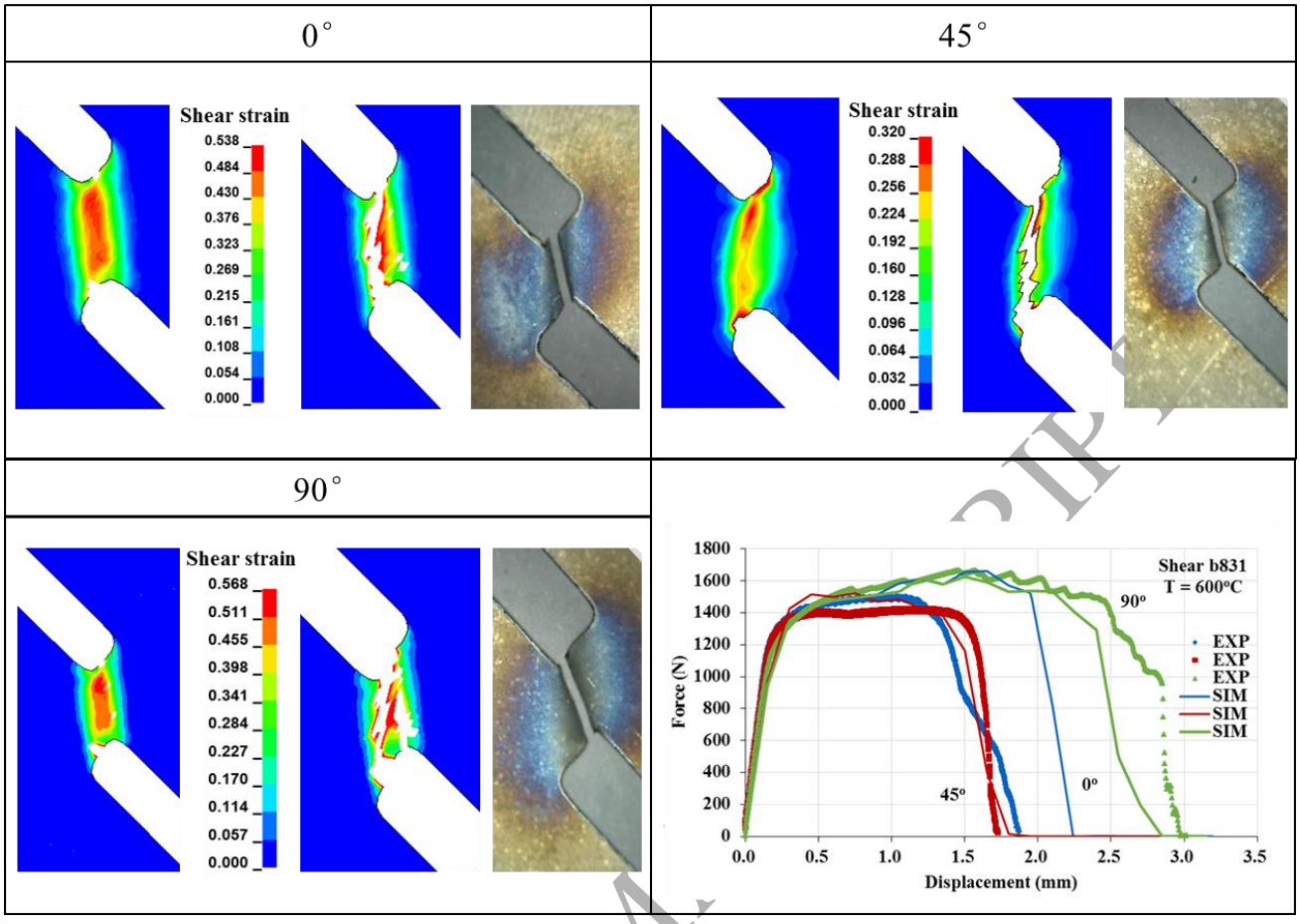

Fig. 14 Experimental and numerically predicted fracture characteristics of shear specimens deformed at 600°C at varying rolling direction.

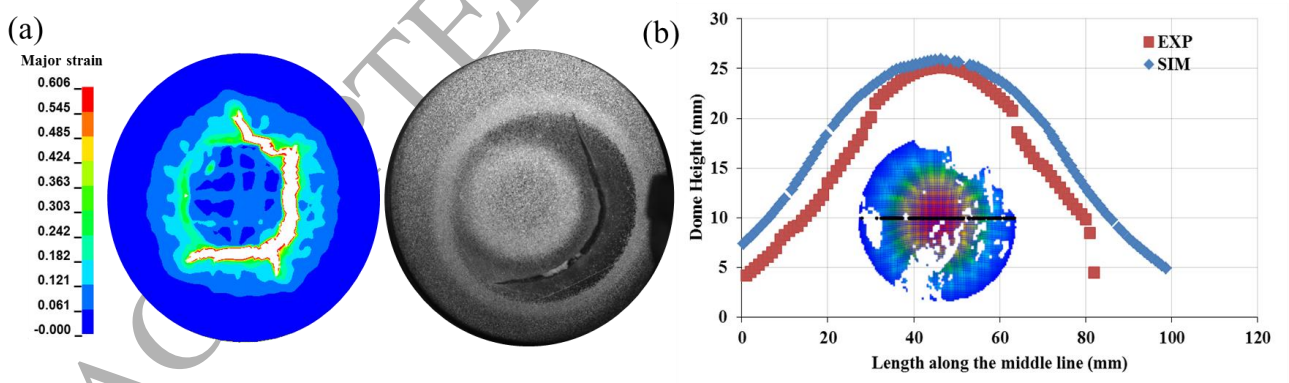

Fig. 15 Experimental and numerically predicted fracture characteristics of Nakajima round specimens deformed at 600°C.

4.4 Modelling validation

The experimental outcomes from testing Nakajima notched specimens, not included in the calibration procedure, were used to validate the modelling approach proposed in §4.2. Figure 16 (a) shows the numerical model used for such test, whereas Figure 16 (b) shows the comparison between the experimental and numerical dome heights. As expected, as a consequence of the material increased ductility, the dome height at room temperature is lower than

the one at 600°C. Both at room temperature and 600°C, the agreement between experimental and numerical results is very satisfactory, with a maximum difference less than 15%. Figure 17 shows the comparison between the experimental and numerically predicted fracture morphology and location at different specimen rolling direction, both at room temperature and 600°C. It is worth noting that the GISSMO model is capable of predicting both the location and fracture shape. Even the tilted crack shape characteristic of the 45° oriented specimen is well predicted.

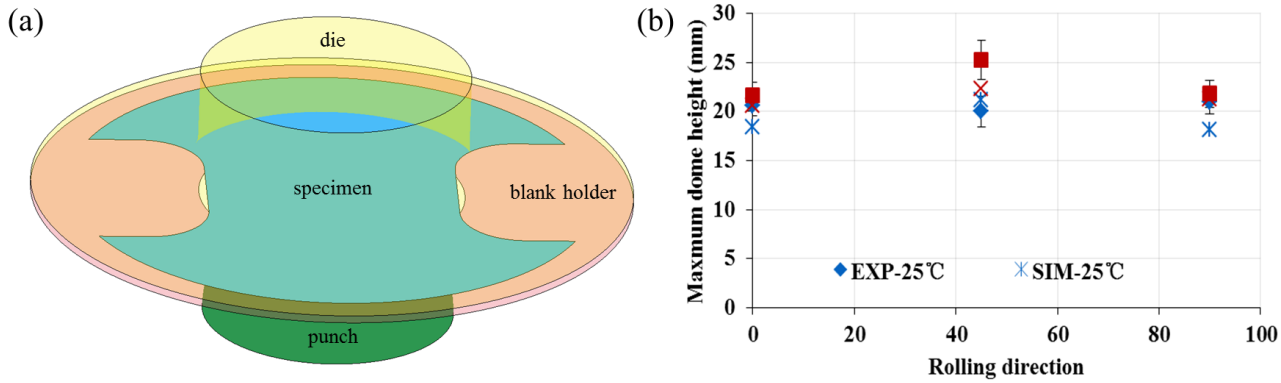

Fig. 16 (a) FE model of the Nakajima set-up for testing notched specimens. (b) Experimental and numerically predicted dome heights at room temperature and 600°C at varying rolling direction.

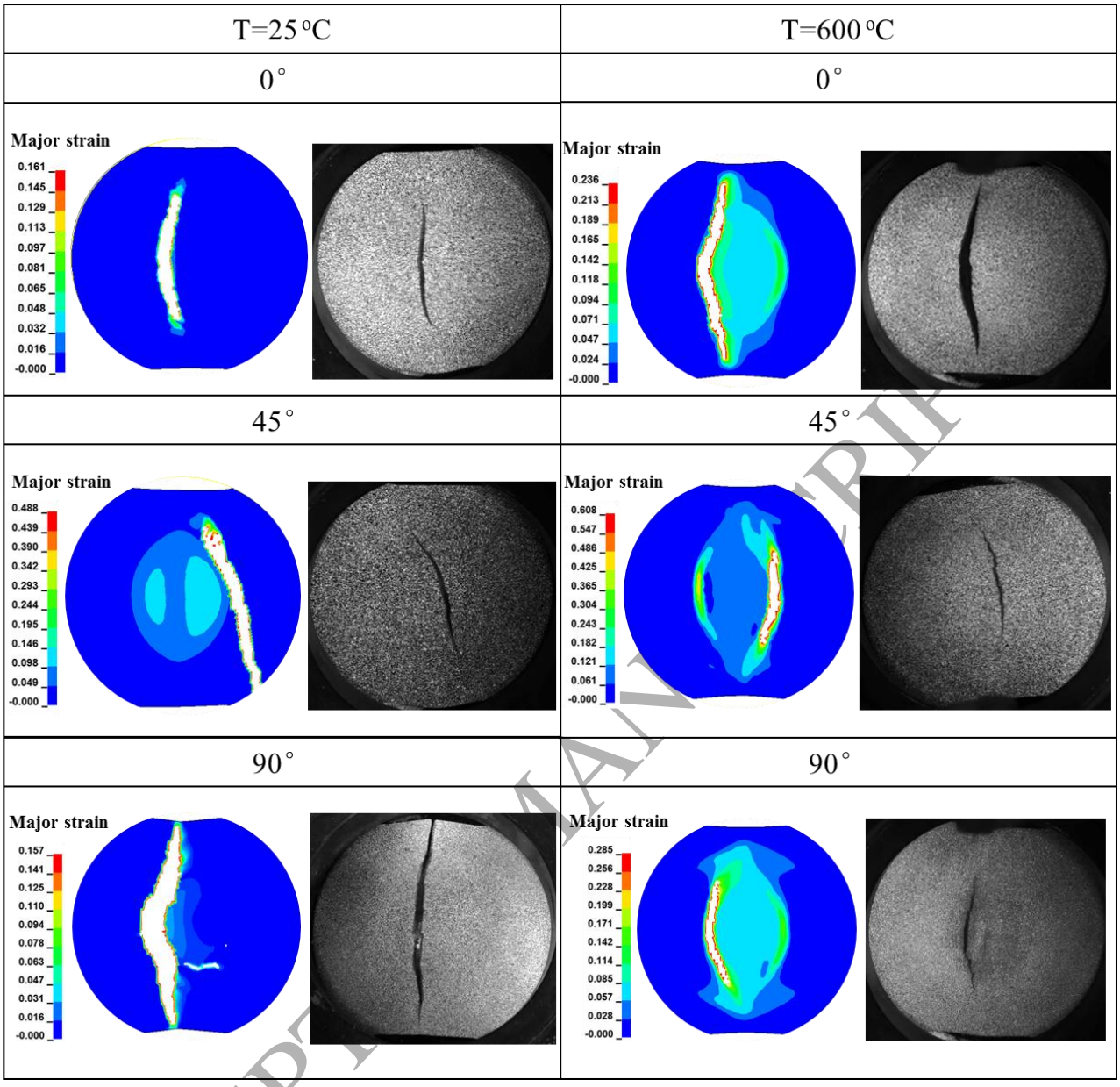

Fig.17 Experimental and numerically predicted fracture characteristics of Nakajima notched specimens deformed at room temperature and 600°C at varying rolling direction.

5. Conclusions

The paper focused on the numerical prediction of ductile failure of Ti6Al4V titanium alloy sheets when deformed at room and elevated temperature taking into account the sheet anisotropic behaviour. In order to do that, the Barlat-Lian 1989 yield criterion and the GISSMO model were used, suitably calibrated on the basis of an extensive experimental campaign that included tensile tests on smooth and notched samples, shear tests and Nakajima-type tests in order to have a wide range of stress triaxiality values. The tests were carried out on specimens machined at different rolling orientation to account for the material anisotropic behaviour. The numerical model was then validated on the basis of the outcomes of tests not included in the calibration phase.

The following conclusions can be drawn:

- The Ti6Al4V sheets retained their anisotropic behaviour till 700°C, being both the strain at fracture and instability strain significantly influenced by the rolling direction at varying stress triaxiality; in particular,

the 45° direction always showed the highest ductility, except in case of shear samples, both at room temperature and 600°C.

- The Barlat-Lian1989 yield criterion was calibrated on the basis of the Lankford coefficients, and the associated hardening rule on the basis of the material flow stress at varying temperature and strain rate, whereas the GISSMO model by means of the strain at fracture and instability strain values at varying stress triaxiality and rolling direction, at room temperature and 600°C.
- The numerical models of the tensile and shear tests with implementations of the calibrated Barlat-Lian 1989 and GISSMO models proved to give a satisfactory agreement with the experimental outcomes, in terms of force vs. displacement curves, strain field, fracture location and characteristics; the same agreement was found in case of Nakajima-type tests in terms of dome height and fracture location and characteristics, considering both the geometry used for calibration and the one for validation.
- The models were, in general, able to catch the differences in fracture occurrence due to the different anisotropic characteristics, with just a slight disagreement in case of 90° oriented specimens, especially under shear conditions, which need further investigations.

Acknowledgments: The financial support of the China Scholarship Council (CSC) (No. 201608370094) is gratefully acknowledged.

References

[1] Monika Jenko, Matevz, Gorensek, Matjaz Godec, Maxinne Hodnik, Barbara Setina Batic, Crtomir Donik, John T. Grant, Drago Dolinar. Surface chemistry and microstructure of metallic biomaterials for hip and knee endoprostheses. Appl Surf Sci. 427 (201584-593. 10.1016/j.apsusc.2017.08.007

[2] J.M. Cordeiro, V.A.R. Barão. Is there scientific evidence favoring the substitution of commercially pure titaniumwith titanium alloys for the manufacture of dental implants? Mater Sci Eng C. 71 (2017) 1201-1215. 10.1016/j.msec.2016.10.025

[3] K.S. Chan, D.A. Koss. Deformation and Fracture of Strongly Textured Ti Alloy Sheets in Uniaxial Tension. Metall Trans. A. 14 (1983) 1333-1342. 10.1007/BF02664816

[4] O.M. Badr, F. Barlat, B. Rolfe. Constitutive modelling of high strength titanium alloy Ti-6Al-4V for sheet forming applications at room temperature. Int J Solids Struct. 80 (2016) 334-347. 10.1016/j.ijsolstr.2015.08.025

[5] N. Kotkunde, A.D. Deole, A.K. Gupta, S.K Singh. Experimental and numerical investigation of anisotropic yield criteria for warm deep drawing of Ti-6Al-4V alloy. Mater Des. 63 (2014) 336-344. 10.1016/j.matdes.2014.06.017

[6] N. Allahverdizadeh, A. Gilioli, A. Manes, M. Giglio. An experimental and numerical study for the damage characterization of Ti-6AL-4V titanium alloy. Int J Mech Sci. 93 (2015) 32-47. 10.1016/j.ijmecsci.2015.01.005

[7] S. Bruschi, T. Altan, D. Banabic, P.F. Bariani, A. Brosius, J. Cao, A. Ghiotti, M. Khraisheh, M. Merklein, A.E. Tekkaya. Testing and modelling of material behaviour and formability in sheet metal forming. CIRP Ann Manuf Technol. 63 (2014) 727-749. 10.1016/j.cirp.2014.05.005

[8] F.X.C. Andrade, M. Feucht, A. Haufe, F. Neukamm. An incremental stress state dependent damage model for ductile failure prediction. Int J Fract. 200 (2016) 127-150. 10.1007/s10704-016-0081-2

[9] D. Hörling. Parameter identification of GISSMO damage model for DOCOL 1200M. Faculty of science and technology. 2015. urn:nbn:se:kau:diva-37417

[10] S. Heibel, W Nester, T Clausmeyer, A.E. Tekkaya. Failure assessment in sheet metal forming using a phenomenological damage model and fracture criterion: experiments, parameter identification and validation. Procedia Eng. 207 (2017) 2066-2071. 10.1016/j.proeng.2017.10.1065

[11] H. Sandberg , O. Rydholm. Evaluation of Material Models to Predict Material Failure in LS-DYNA. Department of Construction Sciences. Division of Solid Mechanics. Lund University. 2016.

[12] ASTM E8/E8M-16a. Standard test methods for tension testing of metallic materials.

[13] B. Valoppi, S. Bruschi, A Ghiotti. Johnson-Cook based criterion incorporating stress triaxiality and deviatoric effect for predicting elevated temperature ductility of titanium alloy sheets. Int J Mech Sci. 123 (2017) 94-105. 10.1016/j.ijmecsci.2017.02.005

[14] ASTM B831. Standard test method for shear testing of thin aluminum alloy products. n.d.

[15] Q.L. Wang, A. Ghiotti, S. Bruschi. Anisotropy Influence on the Failure of Ti6Al4V Sheets Deformed at Room and Elevated Temperature. AIP Conference Proceedings 1960, 160030 (2018). 10.1063/1.5035056

[16] G.J. Oh, K.M. Lee, M.Y. Huh, J.E. Park, S.H. Park, O. Engler. Effect of r-Value and Texture on Plastic Deformation and Necking Behavior in Interstitial-Free Steel Sheets. Met Mater Int. 23 (2017) 26-34. 10.1007/s12540-017-6375-8

[17] ISO 12004-2:2008, TC 164/SC 2. Metallic material-Sheet and strip-Determination of forming limit curves-Part 2: Determination of forming limit curves in the laboratory.

[18] S.K. Singh, K. Mahesh, A. Kumar, M. Swathi. Understanding formability of extra deep drawing steel at elevated temperature using finite element simulation. Mater Des. 31 (2010) 4478-4484. 10.1016/j.matdes.2010.04.049

[19] G. Chandra Mohan Reddy, P.V.R. Ravindra Reddy, T.A. Janardhan Reddy. Finite element analysis of the effect of coefficient of friction on the drawability. Tribol Int. 43 (2010) 1132-1137. 10.1016/j.triboint.2009.12.024

[20] R. Boyer, E.W. Collings, G. Welsch. Materials Properties Handbook: Titanium Alloys. ASM International (1994).

[21] F. Barlat, K. Lian. Plastic behaviour and stretchability of sheet metals (Part I): A yield function for orthotropic sheet under plane stress conditions. Int J Plasticity. 5 (1989) 51-56. 10.1016/0749-6419(89)90019-3

[22] D. Banabic. Plastic Behaviour of Sheet Metal. In: Sheet Metal Forming Processes. Springer, Berlin, Heidelberg. (2010) P. 27-140. 10.1007/978-3-540-88113-1_2

[23] F. Neukamm, M. Feucht, A. Haufe. Considering damage history in crashworthiness simulations. In: Proceedings of the 7th European LS-DYNA users conference. Salzburg. Austria. (2009)

[24] N. Stander, W. J. Roux, T. Goel, T. Eggleston, K.J. Craig, LS_OPT Version 4.1 User's Manual, Livermore Software Technology Corporation, (2010).

[25] N. Stander, K.J. Craig. On the robustness of a simple domain reduction scheme for simulation-based optimization. Eng. Comut. 19 (2002) 431-450. 10.1108/02644400210430190

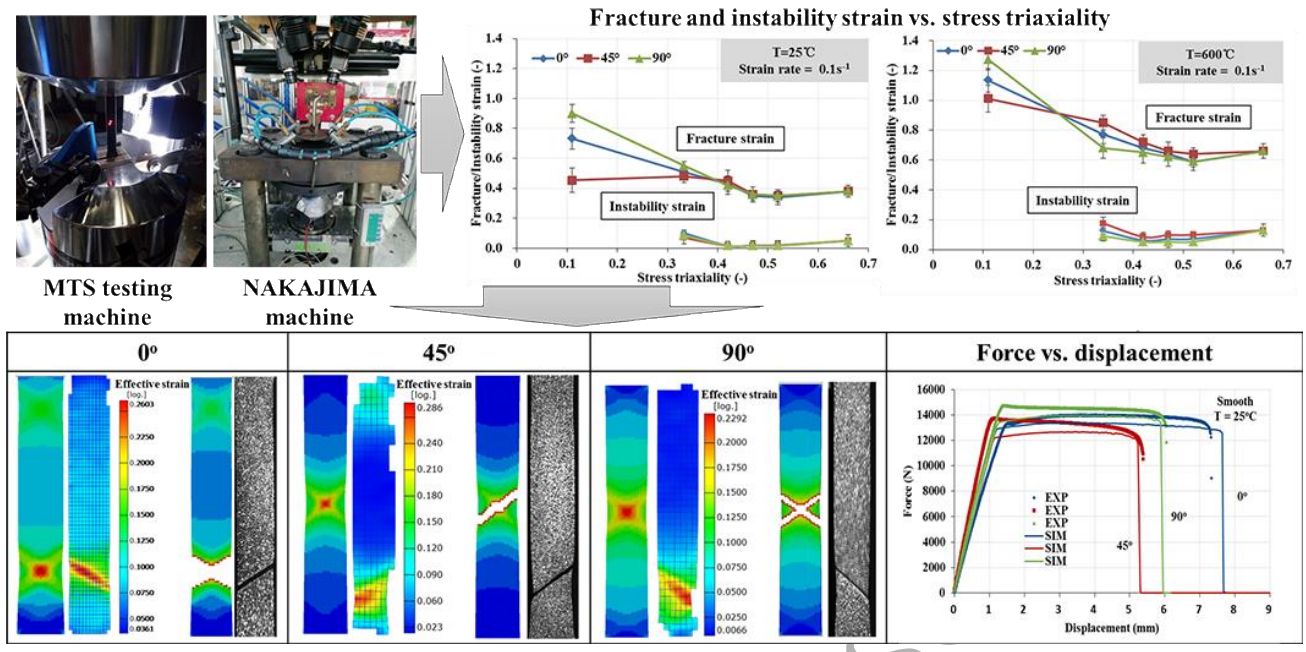

Graphical Abstract